Water Waves (2025) 7:495–519
https://doi.org/10.1007/s42286-025-00123-8

ORIGINAL ARTICLE

Flow of a Periodic Interfacial Travelling Water Wave

Filipe S. Cal[1,2] · **Gonçalo A. S. Dias**[1]

Received: 19 March 2025 / Accepted: 20 June 2025 / Published online: 26 August 2025

Abstract
We consider a symmetric periodic travelling wave propagating at the interface between two homogeneous, incompressible, irrotational and inviscid fluids bounded by horizontal planes. For interfacial waves of small amplitude, we present a formula for the interface wave depending on the pressure at the rigid lid and at the flat bottom, and, for the general non-linear case, we derive a lower bound for the interfacial wave height. Under certain conditions imposed on the horizontal component of the motion at the interface and supposing that the horizontal components of the velocity in each layer never reach the wave speed, we study the monotonicity of the horizontal component of the velocity field along the streamlines and also analyze the monotonicity of the pressure along horizontal lines throughout the fluid in both layers, and along the boundary of the domain, between the crest and the trough. Finally, based on the behavior of the velocity field components, we build a pictorial description of the particle paths in both layers.

Keywords Interfacial waves · Two-layer fluid · Wave height · Particle paths

1 Introduction

Interfacial waves propagate at the interface between two fluids of different densities lying one on top of the other. In one sense, surface waves on the ocean are interfacial waves that propagate at the interface between water and air. However, the difference lies in that the pressure at the surface is assumed constant and the air density null, something that does not happen in general at a general fluid interface.

In 1928, Kotchine [1] was the first to demonstrate the existence of stable, periodic travelling interfacial waves between two confined fluids. Moreover, he showed

✉ Gonçalo A. S. Dias
goncalo.dias@isel.pt

Filipe S. Cal
filipe.cal@isel.pt

[1] Instituto Superior de Engenharia de Lisboa, Instituto Politécnico de Lisboa, Rua Conselheiro Emídio Navarro, 1959-007 Lisbon, Portugal

[2] CIMA-Research Center for Mathematics and Applications, Evora, Portugal

that a solution exists for the problem when the amplitude of the interfacial waves is sufficiently small, extending beyond the research of Levi-Civita [2] and Struik [3].

Holyer [4], in 1979, studied large amplitude, progressive interfacial waves moving between two infinite fluids of different densities, calculating the highest wave using the criterion that it has zero horizontal fluid velocity at the interface in a frame moving at the phase speed of the waves. It was found that as the density ratio increases the maximum height of the wave, for fixed wavelength, increases. The existence of overhanging gravity waves of permanent form at the interface between two fluids of different density was afterwards established by Meiron and Saffman [5], where numerical results which demonstrate their existence were presented.

More recently, Sun [6] proved the existence of interfacial periodic traveling waves of small and large amplitude through global bifurcation theory in a two-dimensional framework, where the flow has no rigid boundaries. In 2010, Camassa et al. [7] studied fully non-linear internal travelling waves propagating in a two-layer fluid system of finite depth. The authors sought periodic wave solutions of the long-wave, strongly non-linear asymptotic model derived by Choi and Camassa [8], for a system of two inviscid and nearly irrotational fluid layers of constant densities under gravity and concluded that these solutions are a five-parameter family.

In 2018, Maklakov and Sharipov [9] studied progressive gravitational waves at the interface between two unbounded fluids of different densities to find almost limiting configurations for the so-called overhanging waves. A numerical method of computing interfacial waves based on the representation of a piecewise-analytic function to be found was developed in such a manner that only the shape of the interface is unknown. Later, in 2021, Guan et al. [10] considering two-dimensional periodic interfacial gravity waves travelling between two homogeneous fluids of finite depth, obtained highly accurate solutions using a boundary-integral-equation method coupled with Fourier expansions of the unknown functions. By studying the global bifurcation mechanism of periodic interfacial waves, the authors found three types of limiting wave profiles.

To obtain information about the waves in the ocean, underwater pressure sensors have long been in use, since they are simple to install, are cost-effective and less likely to be damaged by sea traffic or fishing activities. In 1992, Drennan et al. [11] studied the velocity field under wind waves using an extensive set of measurements taken from a fixed tower. Velocity measurements, made with miniature drag spheres, were compared with linear theory estimates of the orbital velocities obtained from measured surface elevation. Tsai et al. [12] showed that the pressure transfer function for recovering surface waves from underwater pressure should include a transducer submergence parameter as that given by the linear theory. Escher and Schlurmann [13] presented a consistent derivation of the pressure transfer function for small amplitude waves within the framework of linear wave theory and discussed some non-linear aspects.

In 2013, Clamond and Constantin [14] derived an equation relating the pressure at the flat bed and the profile of an irrotational steady water wave, permitting the recovery of the surface wave from pressure measurements at the bed. Then in 2014 Constantin [15] provided some estimates for the wave height of a two-dimensional travelling gravity water wave from pressure measurements at the flat bed, without limitations on the wave amplitude. In 2017, Vasan et al. [16] proposed an operational formulation

for reconstructing a time series of water surface displacement from waves using measurements of pressure. The approach was based on the fully non-linear formulation for pressure below traveling-wave solutions of Euler's equations developed by Oliveras et al. [17]. Bonneton et al. [18], in 2018, derived a non-linear weakly dispersive formula to reconstruct, from pressure measurements, the surface elevation of non-linear waves propagating in shallow water. The formula is local in time and only involves first and second order time derivatives of the measured pressure. This approach was evaluated on laboratory and field data of shoaling waves near the breaking point.

Basu [19] provided some bounds on the estimated wave heights, valid for all ranges of amplitudes from pressure measurements, at the flat bed, for steady water waves flowing over underlying uniform currents. The derived upper bound for the wave height, in the case when the speed of the underlying current is greater than the wave speed, is different from the one when there is no current. Later, Basu [20] obtained estimates of wave heights valid for large amplitudes from pressure and flow measurements at an arbitrary intermediate depth.

More recently, Marino et al. [21] derived formulas to recover wave surface elevation from pressure measurements. The study focused on the formulas' performance in the region where the wave non-linearity gradually increases as the wave travels towards shallower waters. Formulas based on linear wave theory alongside non-linear reconstructions were considered. Murashige and Choi [22] explored basic mechanisms for the instability of finite-amplitude interfacial gravity waves through a two-dimensional linear stability analysis of the periodic and irrotational plane motion of the interface between two unbounded, homogeneous fluids of different density in the absence of background currents. Li et al. [23] presented some wave height estimates for the two-dimensional steady periodic water waves subject to the effect of vorticity. Lower bounds of wave heights for the case of positive vorticity and negative vorticity are derived, respectively. This study also provided some upper bounds of wave heights, which rely on velocity and pressure data at an arbitrary intermediate depth.

In this work, our focus is on symmetric periodic travelling, irrotational waves propagating at the interface between two homogeneous, incompressible and inviscid fluids bounded by horizontal planes. For interfacial waves of small amplitude, we are able to give a formula for the interface function from pressure measurements on the rigid lid and on the flat bottom. However, when the wave amplitude is no longer of small amplitude, the linear approximation breaks down. Finding exact solutions to the governing equations in the fully non-linear case becomes much more difficult. Therefore, for the non-linear case, we derive a lower bound for the interfacial wave height, based on the pressure measurements at the boundaries of the fluid.

Constantin and Villari [24] showed that in the case of linear periodic gravity water waves there are no closed orbits for the fluid particles in the fluid and Constantin [25] proved, in the absence of underlying currents, that this feature holds for Stokes waves of small and large amplitudes. Due to the lack of formulas for the free surface, the trajectories of the fluid particles were described qualitatively and it was shown that each particle experiences (per period) a backward–forward motion that leads overall to a forward drift.

In 2011, Umeyama and Matsuki [26] investigated the motion of internal waves traveling through a two-layer fluid of finite depth, employing particle image velocimetry.

They measured the velocity vector field and the vertical distributions of its components at different points in the wave cycle, then compared these measurements with theoretical predictions based on third-order Stokes internal wave theory. One year later, Borluk and Kalisch [27] explored velocity fields linked to exact solutions of the Korteweg–de Vries (KdV) equation and numerically calculated the corresponding particle trajectories. This work included solitary waves, periodic traveling waves, and two-soliton interactions. For the solitary and periodic wave cases, approximate particle paths were found in closed form.

More recently, in 2021, Bjørnestad et al. [28] examined both Eulerian and Lagrangian measurements of orbital velocities in waves approaching the shore. Their objective was to assess how variations in mean water level, wave height, and incipient wave breaking influence the mass transport characteristics of waves in surf zone.

Assuming certain conditions imposed on the horizontal component of the velocity of the motion at the interface (see Cal and Dias [29]) and supposing that the horizontal components of the velocity in each layer never reach the wave speed, and thus excluding the possibility of overhanging waves (see Holyer [4]), we also study the fluid motion in both layers and derive the particle paths above and below the interfacial waves, extending the results obtained by Constantin [25] and Constantin and Strauss [30].

The paper is organised as follows. In Sect. 2, we introduce the notation and present the equations of motion for a fluid bounded from bellow by a flat bottom and from above by a rigid lid, consisting of two homogeneous, incompressible, irrotational, inviscid fluids, with constant densities, ρ_1 and ρ_2, with $\rho_2 > \rho_1$ for gravitational stability. In Sect. 3, under the linear water wave assumptions, we introduce the linearised equations of motion for a two-layer fluid bounded from below by a flat bottom and from above by a rigid lid and present the solution for this problem. We derive a formula for the interfacial wave depending on the pressure at the rigid lid and at the flat bottom and, for the general non-linear case, we derive a lower bound for the interfacial wave height based on the properties of the velocity field in each layer. In Sect. 4, introducing in each layer a stream function and a potential function, we define the hodograph change of variables, which allows us to rewrite the problem as a non-linear boundary problem in a fixed rectangular domain. Within this framework, we study the monotonicity of the horizontal component of the velocity field along the streamlines and, using the Euler equations, we analyze the monotonicity of the pressure along horizontal lines throughout the fluid in both layers, and along the boundary of the domain, between the crest and the trough, from the lower left corner to the top left corner going anticlockwise. Moreover, we characterize the zero level set of the horizontal component of the velocity field and study the dependence of the slope of the streamlines on the fluid depth. Finally, considering that the *drift* is positive and based on the behavior of the velocity field components, we build a pictorial description of the particle paths in both layers.

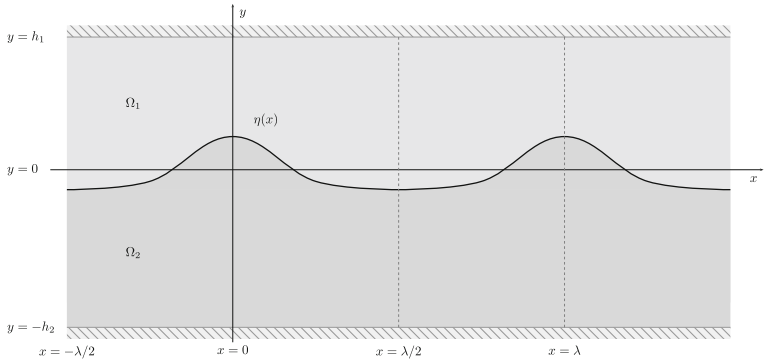

Fig. 1 The fluid domain

2 Formulation of the Problem

The boundary between two semi-infinite fluid layers is represented by an interface defined by a smooth, λ-periodic function $(x, t) \mapsto \eta(x, t)$, which is even and strictly decreasing in the interval $(0, \lambda/2)$ with respect to x. This function satisfies the following condition of zero mean value

$$\int_0^\lambda \eta(x, t)\, \mathrm{d}x = 0, \tag{1}$$

for all time $t \geq 0$. The wave moves with a speed $c > 0$, and we assume that the function representing the interface takes the form $(x, t) \mapsto \eta(x - ct)$, implying that the profile of the interface moves with the fluid in a reference frame moving with speed c. In this new frame, we define two regions

$$\Omega_1 = \{(x, y) \in \mathbb{R}^2 : \eta(x) < y < h_1\},$$

which represents the upper fluid layer, and

$$\Omega_2 = \{(x, y) \in \mathbb{R}^2 : -h_2 < y < \eta(x)\},$$

which represents the lower fluid layer. Here, h_1 and h_2 are positive real numbers that denote the thickness of the upper and lower layers, respectively (Fig. 1).

In each region Ω_j, (for $j = 1, 2$), we define the velocity field $(u^{(j)}, v^{(j)})$ and write down the mass conservation equation

$$u_x^{(j)} + v_y^{(j)} = 0, \tag{2}$$

where subscripts denote partial differentiation. The motion of the fluid is described by the Euler equations for each layer

$$(u^{(j)} - c)u_x^{(j)} + v^{(j)}u_y^{(j)} = -\frac{P_x^{(j)}}{\rho_j}, \tag{3a}$$

$$(u^{(j)} - c)v_x^{(j)} + v^{(j)}v_y^{(j)} = -\frac{P_y^{(j)}}{\rho_j} - g, \tag{3b}$$

where $P^{(j)}$ is the internal pressure in each fluid layer, ρ_j is the density of the fluid in the jth layer, and g is the gravitational acceleration. The interface between the two layers is, in turn, represented by

$$\Gamma = \left\{(x, y) \in \mathbb{R}^2 : \ y = \eta(x)\right\}.$$

At the interface, the transmission boundary conditions are

$$v^{(j)} = (u^{(j)} - c)\,\eta_x, \quad j = 1, 2 \tag{4a}$$

$$P^{(1)} = P^{(2)}, \tag{4b}$$

and tell us that the pressure and the normal velocity are continuous across the interface between the fluid layers. At the rigid lid

$$\Gamma_1 = \left\{(x, y) \in \mathbb{R}^2 : \ y = h_1\right\}$$

and on the flat bottom

$$\Gamma_2 = \left\{(x, y) \in \mathbb{R}^2 : \ y = -h_2\right\},$$

we have the Neumann boundary conditions

$$v^{(j)} = 0 \quad \text{on } \Gamma_j, \qquad j = 1, 2. \tag{5}$$

Assuming that the fluid is irrotational in each layer separately, we find that

$$u_y^{(j)} = v_x^{(j)} \quad \text{in } \Omega_j, \qquad j = 1, 2. \tag{6}$$

In this work, we focus on smooth interfacial waves, which are solutions to the equations (2)–(6), with $u^{(j)}$, $v^{(j)}$ and $P^{(j)}$ being smooth functions with period λ in the x-direction. Additionally, $u^{(j)}$ and $P^{(j)}$ are even functions of x, while $v^{(j)}$ is an odd function of x. It is assumed, moreover, that the horizontal component of the velocity field throughout the fluid, in each layer $u^{(j)}$, is smaller than the wave speed c. This excludes highest waves (see Holyer [4]). In our description, this is captured by imposing the condition

$$u^{(j)} - c < 0 \quad \text{in } \overline{\Omega_j}, \qquad j = 1, 2. \tag{7}$$

On the flat bottom and at the rigid lid, we assume that there are no constant underlying or overlying currents, i.e.,

$$\int_0^\lambda u^{(1)}(x, h_1)\,\mathrm{d}x = 0 \quad \text{and} \quad \int_0^\lambda u^{(2)}(x, -h_2)\,\mathrm{d}x = 0. \tag{8}$$

This condition means that, from a physical point of view, the average motion per wavelength of the fluid is zero at the upper and lower boundaries of the fluid domain.

Finally, along the interface, we assume that $u^{(1)}$ is strictly increasing and $u^{(2)}$ strictly decreasing (as a function of x) from crest to trough (see Cal and Dias [29]), i.e., for all $x \in (0, \lambda/2)$,

$$\partial_x u^{(1)}(x, \eta(x)) > 0 \quad \text{and} \quad \partial_x u^{(2)}(x, \eta(x)) < 0. \tag{9}$$

3 Interfacial Wave Profile

The simplest approximation for the profile of a periodic travelling interfacial wave between two bounded fluids, with known rigid lid $P^{(1)}(x, h_1)$ and bottom wall pressure $P^{(2)}(x, -h_2)$, is obtained by considering the undisturbed flow $(u^{(j)}, v^{(j)}) = (c, 0)$. From the Euler equations (3), making use of the boundary condition (4b) at the interface, we immediately arrive at

$$\eta(x) = \frac{P^{(2)}(x, -h_2) - P^{(1)}(x, h_1)}{g(\rho_2 - \rho_1)} - \frac{\rho_2 h_2 + \rho_1 h_1}{\rho_2 - \rho_1}, \tag{10}$$

for all $x \in \mathbb{R}$.

3.1 Linear Water Wave Approximation

Assuming that the wave motion is of small amplitude (wave height is much smaller than the water depth) and of small slope (wave height is much smaller than the wave length), the equations of motion can be linearized for a two-layer fluid bounded above by a rigid lid as

$$\begin{aligned}
&u_x^{(j)} + v_y^{(j)} = 0 \quad \text{in } \Omega_j^L, \qquad j = 1, 2,\\
&-c\,u_x^{(j)} = -\frac{P_x^{(j)}}{\rho_j} \quad \text{in } \Omega_j^L, \qquad j = 1, 2,\\
&-c\,v_x^{(j)} = -\frac{P_y^{(j)}}{\rho_j} - g \quad \text{in } \Omega_j^L, \qquad j = 1, 2,
\end{aligned} \tag{11}$$

where

$$\Omega_1^L = \{(x, y) \in \mathbb{R}^2 : 0 < y < h_1\} \quad \text{and} \quad \Omega_2^L = \{(x, y) \in \mathbb{R}^2 : -h_2 < y < 0\}.$$

At the rest position of the interface, $y = 0$, we get

$$\begin{aligned} v^{(j)} &= -c\,\eta_x, \quad j = 1, 2 \\ P^{(1)} - \rho_1\, g\, \eta &= P^{(2)} - \rho_2\, g\, \eta. \end{aligned} \tag{12}$$

On the rigid lid and on the flat bottom, we have the Neumann boundary conditions

$$\begin{aligned} v^{(1)} &= 0, \quad y = h_1, \\ v^{(2)} &= 0, \quad y = -h_2. \end{aligned} \tag{13}$$

Using the *ansatz*

$$\eta(x) = a\cos(kx), \tag{14}$$

where $k = \frac{2\pi}{\lambda}$ denotes the wave number and $a \in \mathbb{R}$ the amplitude of the interface, we obtain (see Cal and Dias [29]) the following solution for the linearized problem (11)–(13):

$$\begin{aligned} u^{(1)}(x, y) &= -ack\frac{\cosh(k(y - h_1))}{\sinh kh_1}\cos kx, \\ v^{(1)}(x, y) &= -ack\frac{\sinh(k(y - h_1))}{\sinh kh_1}\sin kx, \\ u^{(2)}(x, y) &= ack\frac{\cosh(k(y + h_2))}{\sinh kh_2}\cos kx, \\ v^{(2)}(x, y) &= ack\frac{\sinh(k(y + h_2))}{\sinh kh_2}\sin kx, \end{aligned}$$

satisfying the dispersion relation

$$c^2 = \frac{g(\rho_2 - \rho_1)}{k(\rho_1 \coth kh_1 + \rho_2 \coth kh_2)}. \tag{15}$$

Proposition 3.1 *For waves of small amplitude, i.e., solutions of the linearised problem* (11)–(13)*, the periodic function* η *representing the interface profile between the two fluid layers, depending on the pressure at the rigid lid and at the flat bottom, in the moving reference frame with speed* c*, is given by*

$$\eta(x) = \left(\frac{\rho_1 \coth kh_1 + \rho_2 \coth kh_2}{\rho_1\ \mathrm{csch}\, kh_1 + \rho_2\ \mathrm{csch}\, kh_2}\right)\frac{P^{(2)}(x, -h_2) - P^{(1)}(x, h_1) - \rho_2 g h_2 - \rho_1 g h_1}{g(\rho_2 - \rho_1)}, \tag{16}$$

for all $x \in \mathbb{R}$.

Proof In view of Eq. (11), we arrive at

$$\frac{P^{(1)}(x,y)}{\rho_1} = -c^2 k \frac{\cosh(k(y-h_1))}{\sinh kh_1}\eta(x) - gy + \tilde{P}_1,$$
$$\frac{P^{(2)}(x,y)}{\rho_2} = c^2 k \frac{\cosh(k(y+h_2))}{\sinh kh_2}\eta(x) - gy + \tilde{P}_2,$$

$\tilde{P}_1, \tilde{P}_1 \in \mathbb{R}$. The previous equations at the rest position of the interface $y = 0$ read as

$$\frac{P^{(1)}(x,0)}{\rho_1} = -c^2 k \coth kh_1\, \eta(x) + \tilde{P}_1,$$
$$\frac{P^{(2)}(x,0)}{\rho_2} = c^2 k \coth kh_2\, \eta(x) + \tilde{P}_2,$$

and considering Eq. (12), it follows

$$\eta(x)\left(c^2 k(\rho_1 \coth kh_1 + \rho_2 \coth kh_2) - g(\rho_2 - \rho_1)\right) = \rho_1\tilde{P}_1 - \rho_2\tilde{P}_2.$$

From the dispersion relation (15), we can conclude that

$$\rho_1\tilde{P}_1 = \rho_2\tilde{P}_2.$$

By subtracting the pressure at the lid from the one at the bottom and considering the previous equation, the interface profile η reads as

$$\eta(x) = \frac{P^{(2)}(x,-h_2) - P^{(1)}(x,h_1) - \rho_2 g h_2 - \rho_1 g h_1}{c^2 k(\rho_1\ \mathrm{csch}\, kh_1 + \rho_2\ \mathrm{csch}\, kh_2)}$$

and, using the dispersion relation, it can be written as

$$\eta(x) = K\ \frac{P^{(2)}(x,-h_2) - P^{(1)}(x,h_1) - \rho_2 g h_2 - \rho_1 g h_1}{g(\rho_2 - \rho_1)},$$

where

$$K = \frac{\rho_1 \coth kh_1 + \rho_2 \coth kh_2}{\rho_1\ \mathrm{csch}\, kh_1 + \rho_2\ \mathrm{csch}\, kh_2}$$

is a positive constant greater than unity ($K > 1$). □

In view of the previous proposition, evaluating the function η at $x = 0$ and $x = \lambda/2$, we immediately see that the interfacial wave height $H = \eta(0) - \eta(\lambda/2)$ is

$$H = K\ \frac{P^{(2)}(0,-h_2) - P^{(2)}(\lambda/2,-h_2) + (P^{(1)}(\lambda/2,h_1) - P^{(1)}(0,h_1))}{g(\rho_2 - \rho_1)}.$$

Moreover, note that the hydrostatic approximation (10) can be recovered from the linear approximation (16) in the limit $kh_1 \to 0$ and $kh_2 \to 0$.

3.2 Estimating the Wave Height from Below

For the general case, the linear theory is no longer appropriate to describe the wave profile. This makes it much harder to deduce suitable formulas for that profile in the non-linear case. In this section, following the idea of Constantin [15], we derive a lower bound for the interfacial wave height, for the general non-linear case, based on the pressure measurements at the top and bottom boundaries of the fluid.

Proposition 3.2 *For smooth periodic travelling interfacial waves, i.e., solutions of the non-linear problem* (2)–(7)*, the following estimate for the interfacial wave height holds*

$$\eta(0)-\eta(\lambda/2) > \frac{P^{(2)}(0,-h_2) - P^{(2)}(\lambda/2,-h_2)+(P^{(1)}(\lambda/2,h_1) - P^{(1)}(0,h_1))}{g(\rho_2-\rho_1)}. \tag{17}$$

Proof Since $\eta_x(x) < 0$, for all $x \in (0,\lambda/2)$, and $u^{(j)} - c < 0$ in $\overline{\Omega_j}$, by Eq. (4a), we can see that $v^{(j)} > 0$ at the interface. Consequently, noting that $v^{(j)}$ is harmonic and vanishes on the flat bottom and on the rigid lid, it follows that, for $0 < x < \lambda/2$,

$$\begin{cases} v^{(1)}(x,y) > 0, & \eta(x) < y < h_1 \\ v^{(2)}(x,y) > 0, & -h_2 < y < \eta(x) \end{cases}. \tag{18}$$

Furthermore, the Hopf's maximum principle yields

$$v_y^{(1)}(x,h_1) < 0 \quad \text{and} \quad v_y^{(2)}(x,-h_2) > 0, \tag{19}$$

for $x \in (0,\lambda/2)$. On the other hand, taking into account that $v^{(j)}$ is odd and periodic with respect to the x variable, it follows that $v^{(j)}(0,y) = v^{(j)}(\lambda/2,y) = 0$. Consequently, for $-h_2 < y < h_1$,

$$v_x^{(j)}(0,y) > 0 \quad \text{and} \quad v_x^{(j)}(\lambda/2,y) < 0. \tag{20}$$

Considering that the fluid is layerwise incompressible and irrotational, Eq. (19) read as

$$u_x^{(1)}(x,h_1) > 0 \quad \text{and} \quad u_x^{(2)}(x,-h_2) < 0 \qquad \text{for } x \in (0,\lambda/2) \tag{21}$$

and Eq. (20) become

$$u_y^{(j)}(0,y) > 0 \quad \text{and} \quad u_y^{(j)}(\lambda/2,y) < 0 \qquad \text{for } y \in (-h_2,h_1). \tag{22}$$

Now, from the Euler equations (3), we arrive in each fluid layer at Bernoulli's law, which states that the total energy

$$E_j = \rho_j \frac{(u^{(j)} - c)^2 + (v^{(j)})^2}{2} + \rho_j g y + P^{(j)}, \quad j = 1, 2 \tag{23}$$

is constant in the fluid domain Ω_j. In the upper layer, evaluating this equation at the interface and on the rigid lid, at $x = 0$ and $x = \lambda/2$, in view of the inequalities (22) and recalling that $u^{(j)} < c$ in $\overline{\Omega_j}$, we arrive at

$$\eta(0) - h_1 < \frac{P^{(1)}(0, h_1) - P^{(1)}(0, \eta(0))}{g\rho_1}$$

and

$$\eta(\lambda/2) - h_1 > \frac{P^{(1)}(\lambda/2, h_1) - P^{(1)}(\lambda/2, \eta(\lambda/2))}{g\rho_1}.$$

Similarly, in the lower layer, evaluating the Bernoulli's law (23) at the interface and on the flat bottom, at $x = 0$ and $x = \lambda/2$, we get

$$\eta(0) + h_2 > \frac{P^{(2)}(0, -h_2) - P^{(2)}(0, \eta(0))}{g\rho_2}$$

and

$$\eta(\lambda/2) + h_2 < \frac{P^{(2)}(\lambda/2, -h_2) - P^{(2)}(\lambda/2, \eta(\lambda/2))}{g\rho_2}.$$

Considering now that $P^{(1)} = P^{(2)}$ at the interface, we obtain

$$\eta(0) + \frac{\rho_1 h_1 + \rho_2 h_2}{\rho_2 - \rho_1} > \frac{P^{(2)}(0, -h_2) - P^{(1)}(0, h_1)}{g(\rho_2 - \rho_1)}$$

and

$$\eta(\lambda/2) + \frac{\rho_1 h_1 + \rho_2 h_2}{\rho_2 - \rho_1} < \frac{P^{(2)}(\lambda/2, -h_2) - P^{(1)}(\lambda/2, h_1)}{g(\rho_2 - \rho_1)}$$

and, consequently, we obtain the following estimate for the interfacial wave height

$$\eta(0) - \eta(\lambda/2) > \frac{P^{(2)}(0, -h_2) - P^{(2)}(\lambda/2, -h_2) + (P^{(1)}(\lambda/2, h_1) - P^{(1)}(0, h_1))}{g(\rho_2 - \rho_1)}.$$

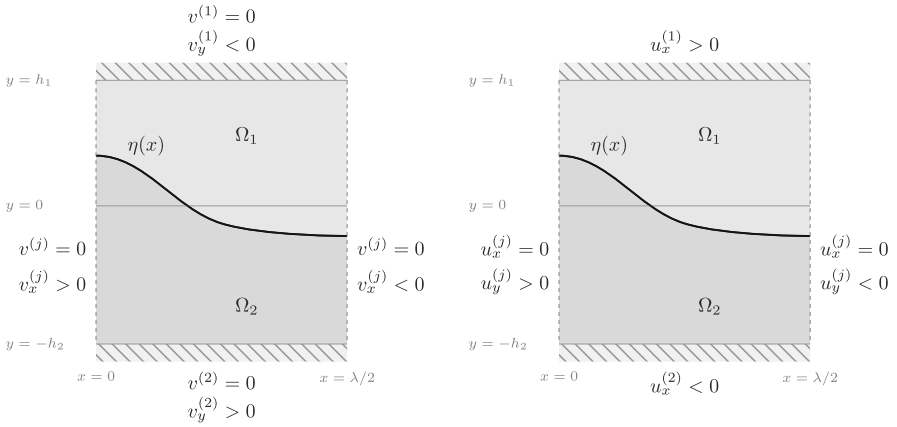

Fig. 2 The vertical $v^{(j)}$ and the horizontal $u^{(j)}$ components of the velocity field

Taking into account the Neumann boundary condition (5) and the inequality (7), and considering that

$$u_x^{(1)}(x, h_1) > 0 \quad \text{and} \quad u_x^{(2)}(x, -h_2) < 0 \qquad \text{for } x \in (0, \lambda/2),$$

from Euler equation (3a), we can see that

$$P_x^{(1)}(x, h_1) > 0 \quad \text{and} \quad P_x^{(2)}(x, -h_2) < 0 \qquad \text{for } x \in (0, \lambda/2).$$

Consequently,

$$P^{(1)}(\lambda/2, h_1) - P^{(1)}(0, h_1) > 0 \quad \text{and} \quad P^{(2)}(0, -h_2) - P^{(2)}(\lambda/2, -h_2) > 0,$$

which allows us conclude that the estimate (17) provides a positive lower bound for the height of the interfacial wave. □

From the previous proposition, it is also noteworthy that the closer the densities, the higher the lower bound (Fig. 2). This happens also in the case of the linear water waves approximation (16), where the amplitude of the interfacial wave is greater the closer the densities and smaller if they differ greatly. This is a consequence of the fact that, with closer densities, the fluid elements on each side of the interface have similar inertia, whereas if the densities are dissimilar the lower fluid will be much denser than the fluid above, with the consequent higher inertia for a fluid element of the former.

Remark 3.1 Since along an interface between two fluid layers the pressure is not necessarily constant, and additionally, given that the function $P^{(1)}$ representing the pressure in the upper layer is superharmonic, the methods used in [15] to obtain an upper bound for a surface wave height couldn't apply to the case of an interfacial wave.

4 Motion Described by a Stream Function

Having obtained the wave profile for the interface η in the linear case and a lower bound on the amplitude of the interfacial wave in the non-linear case, we now set out to determine the streamlines and particle paths in the same setting of a two-layer fluid limited above by a rigid lid and below by a bottom wall. For this purpose, equations (2)–(6) can be rewritten in a more suitable way. Since the fluid is layerwise incompressible, we can introduce, up to a constant, in each layer, the stream function $\psi^{(j)}$ satisfying

$$\psi_y^{(j)} = u^{(j)} - c \quad \text{and} \quad \psi_x^{(j)} = -v^{(j)}, \qquad j = 1, 2. \tag{24}$$

Moreover, Neumann boundary condition (5) and Eq. (4a) imply that the stream functions $\psi^{(j)}$, $j = 1, 2$, are constant at the rigid surfaces Γ_1, Γ_2 and at the interface Γ. Setting $\psi^{(1)} = \psi^{(2)} = 0$ at the interface, we can write the stream functions as

$$\psi^{(1)}(x, y) = -\frac{m_1}{\rho_1} - \int_y^{h_1} \left(u^{(1)}(x, s) - c\right) \mathrm{d}s, \tag{25a}$$

$$\psi^{(2)}(x, y) = \frac{m_2}{\rho_2} + \int_{-h_2}^{y} \left(u^{(2)}(x, s) - c\right) \mathrm{d}s, \tag{25b}$$

where

$$m_1 = -\rho_1 \int_{\eta(x)}^{h_1} \left(u^{(1)}(x, s) - c\right) \mathrm{d}s \quad \text{and} \quad m_2 = -\rho_2 \int_{-h_2}^{\eta(x)} \left(u^{(2)}(x, s) - c\right) \mathrm{d}s, \tag{26}$$

denote the mass flux of the fluid motion in each layer. These quantities are positive, cf. (7), and invariant of the flow. Finally, from Eq. (3), we arrive in each fluid layer at Bernoulli's law, which states that the total energy

$$E_j = \rho_j \frac{\left(\psi_x^{(j)}\right)^2 + \left(\psi_y^{(j)}\right)^2}{2} + \rho_j g y + P^{(j)}, \quad j = 1, 2 \tag{27}$$

is constant in the fluid domain Ω_j and, from the boundary condition (4b) at the interface Γ, it follows that

$$\frac{\rho_2 |\nabla \psi^{(2)}|^2 - \rho_1 |\nabla \psi^{(1)}|^2}{2} + (\rho_2 - \rho_1) g y = E_2 - E_1 \quad \text{on } y = \eta(x). \tag{28}$$

The equations of motion (2)–(6) can now be rewritten as the following free boundary problem

$$\Delta \psi^{(j)} = 0 \quad \text{in } \Omega_j, \qquad j = 1, 2, \tag{29a}$$

$$\psi^{(1)} = -\frac{m_1}{\rho_1} \quad \text{on } \Gamma_1, \tag{29b}$$

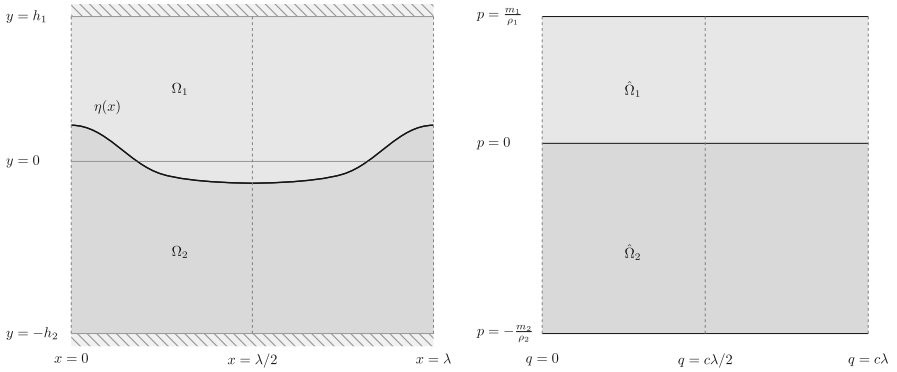

Fig. 3 Hodograph change of variables

$$\psi^{(2)} = \frac{m_2}{\rho_2} \quad \text{on } \Gamma_2, \tag{29c}$$

$$\psi^{(j)} = 0 \quad \text{on } y = \eta(x), \qquad j = 1, 2, \tag{29d}$$

$$\frac{\rho_2|\nabla\psi^{(2)}|^2 - \rho_1|\nabla\psi^{(1)}|^2}{2} + (\rho_2 - \rho_1)gy = E \quad \text{on } y = \eta(x), \tag{29e}$$

where $E = E_2 - E_1$ is a constant.

4.1 Hodograph Transformation

The layerwise irrotationality of the fluid guarantees the existence of a velocity potential $\phi^{(j)}$ in each layer defined, up to a constant, by

$$\phi_x^{(j)} = u^{(j)} - c \quad \text{and} \quad \phi_y^{(j)} = v^{(j)}, \qquad j = 1, 2. \tag{30}$$

Fixing $\phi^{(1)} = \phi^{(2)} = 0$ at the line $x = 0$, we get

$$\phi^{(1)}(x, y) = \int_0^x \left(u^{(1)}(l, h_1) - c\right) \mathrm{d}l - \int_y^{h_1} v^{(1)}(x, s)\, \mathrm{d}s, \tag{31a}$$

$$\phi^{(2)}(x, y) = \int_0^x \left(u^{(2)}(l, -h_2) - c\right) \mathrm{d}l + \int_{-h_2}^y v^{(2)}(x, s)\, \mathrm{d}s. \tag{31b}$$

Since $\phi^{(j)}$ and $\psi^{(j)}$ satisfy Cauchy–Riemann equations in the connected open set Ω_j

$$\begin{cases} \phi_x^{(j)} = \psi_y^{(j)} \\ \phi_y^{(j)} = -\psi_x^{(j)}, \end{cases} \quad j = 1, 2,$$

the function $(x, y) \mapsto \phi(x, y)^{(j)} + \mathrm{i}\psi(x, y)^{(j)}$ is analytic and the velocity potential $\phi^{(j)}$ is harmonic in Ω_j, $j = 1, 2$ (Fig. 3). We can now introduce the conformal map

$H : \Omega_1 \cup \Omega_2 \to \hat{\Omega}_1 \cup \hat{\Omega}_2$, where $(q, p) \in \hat{\Omega}_j$ is defined by

$$\begin{cases} q = -\phi^{(j)}(x, y) \\ p = -\psi^{(j)}(x, y) \end{cases}, \quad \forall (x, y) \in \Omega_j \tag{32}$$

and

$$\hat{\Omega}_1 = \left\{ (q, p) \in \mathbb{R}^2 : 0 < p < \frac{m_1}{\rho_1} \right\}, \quad \hat{\Omega}_2 = \left\{ (q, p) \in \mathbb{R}^2 : -\frac{m_2}{\rho_2} < p < 0 \right\}.$$

The map H transforms the free boundary problem (29) into the following non-linear problem for the harmonic function $h(q, p) = y$ defined in the domain $\hat{\Omega}_1 \cup \hat{\Omega}_2$

$$\Delta_{qp} h = 0 \quad \text{in } \hat{\Omega}_1 \cup \hat{\Omega}_2, \tag{33a}$$

$$h = h_1 \quad \text{on } p = \frac{m_1}{\rho_1}, \tag{33b}$$

$$h = -h_2 \quad \text{on } p = -\frac{m_2}{\rho_2}, \tag{33c}$$

$$\frac{\rho_2}{2} \frac{1}{\left(h_p^{(2)}\right)^2 + \left(h_q^{(2)}\right)^2} - \frac{\rho_1}{2} \frac{1}{\left(h_p^{(1)}\right)^2 + \left(h_q^{(1)}\right)^2} + (\rho_2 - \rho_1) g h = E \quad \text{on } p = 0. \tag{33d}$$

Note that, for $(q, p) \in \hat{\Omega}_j$ and $(x, y) \in \Omega_j$ such that $(q, p) = H(x, y)$, $j = 1, 2$, we have the following equalities:

$$\begin{aligned} \partial_y &= -v^{(j)} \partial_q - (u^{(j)} - c) \partial_p, \\ \partial_x &= -(u^{(j)} - c) \partial_q + v^{(j)} \partial_p, \end{aligned} \tag{34}$$

and

$$\begin{aligned} \partial_q &= h_p^{(j)} \partial_x + h_q^{(j)} \partial_y, \\ \partial_p &= -h_q^{(j)} \partial_x + h_p^{(j)} \partial_y, \end{aligned} \tag{35}$$

where

$$\begin{aligned} h_q^{(j)} &= -\frac{v^{(j)}}{(u^{(j)} - c)^2 + \left(v^{(j)}\right)^2}, \\ h_p^{(j)} &= -\frac{u^{(j)} - c}{\left(u^{(j)} - c\right)^2 + \left(v^{(j)}\right)^2}. \end{aligned} \tag{36}$$

Making use of the hodograph change of variables and taking into account the monotonic conditions (9) imposed on $u^{(j)}$ (as a function of x) along the interface, we generalize below the work of Constantin [31] and Constantin and Strauss [30], by proving some results on the monotonicity of the horizontal component of the velocity field along the streamlines and analyzing the monotonicity of the pressure

along horizontal lines throughout the fluid in both layers, and along the boundary of the domain, between the crest and the trough.

Proposition 4.1 *From the crest to the trough, i.e, for all* $x \in (0, \lambda/2)$,

1. *The horizontal component of the velocity* $u^{(1)}$ *is strictly increasing* (*as a function of* x) *along every streamline* $\psi^{(1)} = -p$, $0 \leq p \leq m_1/\rho_1$.
2. *The horizontal component of the velocity* $u^{(2)}$ *is strictly decreasing* (*as a function of* x) *along every streamline* $\psi^{(2)} = -p$, $-m_2/\rho_2 \leq p \leq 0$.

Proof In the moving framework, considering a streamline parametrized by $x \mapsto (x, \gamma(x))$, $x \in (0, \lambda/2)$, where γ is a differentiable function, we have, by definition,

$$\partial_x\big(\psi^{(j)}(x, \gamma(x))\big) = 0, \quad j = 1, 2.$$

Consequently, on $y = \gamma(x)$, it follows that

$$\psi_x^{(j)} + \psi_y^{(j)}\gamma' = 0$$

and using (24) and (36), we obtain

$$\gamma' = \frac{v^{(j)}}{u^{(j)} - c} = \frac{h_q^{(j)}}{h_p^{(j)}}, \quad j = 1, 2. \tag{37}$$

Therefore, the derivative of $u^{(j)}$ along the streamline, in view of the equalities (35) and (36), can be written as

$$\begin{aligned}\partial_x\big(u^{(j)}(x, \gamma(x))\big) &= u_x^{(j)} + u_y^{(j)}\gamma' = u_x^{(j)} + u_y^{(j)}\frac{h_q^{(j)}}{h_p^{(j)}} \\ &= \frac{u_x^{(j)}h_p^{(j)} + u_y^{(j)}h_q^{(j)}}{h_p^{(j)}} = \frac{u_q^{(j)}}{h_p^{(j)}} \\ &= -u_q^{(j)}\frac{\big(u^{(j)} - c\big)^2 + \big(v^{(j)}\big)^2}{u^{(j)} - c}.\end{aligned} \tag{38}$$

At the crest line $x = 0$ ($q = 0$) and at the trough line $x = \lambda/2$ ($q = c\lambda/2$), since $v^{(j)}$ is periodic and odd with respect to the x variable, we know that $v^{(j)} = 0$ and, consequently, $u_x^{(j)} = -v_y^{(j)} = 0$ at these lines. Thus,

$$u_q^{(j)} = h_p^{(j)}u_x^{(j)} + h_q^{(j)}u_y^{(j)} = 0.$$

On the rigid lid $y = h_1$ ($p = m_1/\rho_1$), by (21) we have $u_x^{(1)}(x, h_1) > 0$ and recalling that $u^{(j)} - c < 0$ in $\overline{\Omega_j}$, $j = 1, 2$, we conclude that

$$u_q^{(1)} = h_p^{(1)}u_x^{(1)} + h_q^{(1)}u_y^{(1)} = -\frac{u^{(1)} - c}{\big(u^{(1)} - c\big)^2 + \big(v^{(1)}\big)^2}u_x^{(1)} > 0.$$

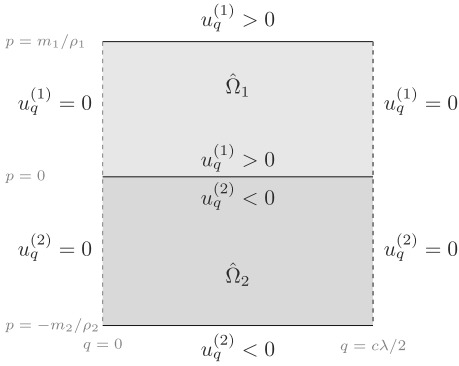

Fig. 4 The harmonic function $u_q^{(j)}$ with respect to the hodograph variables

On the other hand, at the flat bottom $y = -h_2$ ($p = -m_2/\rho_2$), using again the inequality (21), we have $u_x^{(2)}(x, -h_2) < 0$, and, therefore,

$$u_q^{(2)} = h_p^{(2)} u_x^{(2)} + h_q^{(2)} u_y^{(2)} = -\frac{u^{(2)} - c}{\left(u^{(2)} - c\right)^2 + \left(v^{(2)}\right)^2} u_x^{(2)} < 0.$$

At the interface $y = \eta(x)$, for all $x \in (0, \lambda/2)$, ($p = 0$), using the boundary condition (4a), we get

$$\begin{aligned} u_q^{(j)} = h_p^{(j)} u_x^{(j)} + h_q^{(j)} u_y^{(j)} &= -\frac{u^{(j)} - c}{\left(u^{(j)} - c\right)^2 + \left(v^{(j)}\right)^2} u_x^{(j)} - \frac{v^{(j)}}{(u^{(j)} - c)^2 + \left(v^{(j)}\right)^2} u_y^{(j)} \\ &= -\frac{u^{(j)} - c}{\left(u^{(j)} - c\right)^2 + \left(v^{(j)}\right)^2} \left(u_x^{(j)} - \eta_x u_y^{(j)}\right) \\ &= -\frac{u^{(j)} - c}{\left(u^{(j)} - c\right)^2 + \left(v^{(j)}\right)^2} \partial_x \left(u^{(j)}(x, \eta(x))\right) \end{aligned}$$

and, taking into account the monotonic conditions (9) imposed on $u^{(j)}$ (as a function of x), we conclude that, at the interface ($p = 0$), for all $q \in (0, c\lambda/2)$,

$$u_q^{(1)} > 0 \quad \text{and} \quad u_q^{(2)} < 0. \tag{39}$$

Now, by a direct computation, we can see that the function $u^{(j)}$ is harmonic with respect to the hodograph variables, and therefore the function $u_q^{(j)}$ is also harmonic in the (q, p) variables (Fig. 4). Consequently, by the maximum principle for harmonic functions,

$$u_q^{(1)} > 0 \quad \text{in } \{(q, p) \in \mathbb{R}^2 : 0 < q < c\lambda/2 \wedge 0 \le p \le m_1/\rho_1\} \tag{40a}$$

and

$$u_q^{(2)} < 0 \quad \text{in } \{(q, p) \in \mathbb{R}^2 : 0 < q < c\lambda/2 \wedge -m_2/\rho_2 \le p \le 0\}, \tag{40b}$$

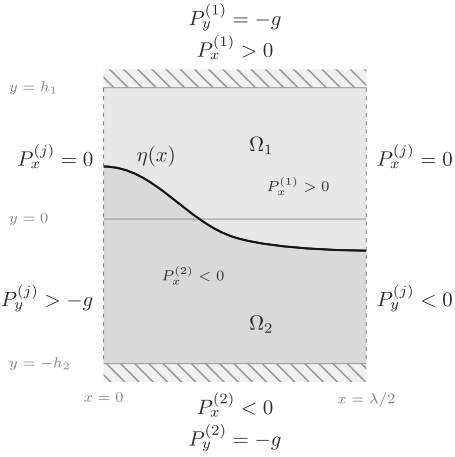

Fig. 5 The function $P^{(j)}$ representing the pressure in the domain

which allow us to conclude, by the equality (38), that, for all $x \in (0, \lambda/2)$,

$$\partial_x\big(u^{(1)}(x, \gamma(x))\big) > 0 \quad \text{and} \quad \partial_x\big(u^{(2)}(x, \gamma(x))\big) < 0.$$

□

Corollary 4.1 *From the crest to the trough, i.e, for all* $x \in (0, \lambda/2)$, $P_x^{(1)} > 0$ *and* $P_x^{(2)} < 0$. *Furthermore* $P_x^{(j)} = 0$ *at the crest line* $x = 0$ *and at the trough line* $x = \lambda/2$, $j = 1, 2$.

Proof Using Euler equation (3a) and the hodograph coordinates,

$$\frac{P_x^{(j)}}{\rho_j} = (c - u^{(j)})u_x^{(j)} - v^{(j)}u_y^{(j)} = \frac{h_p u_x^{(j)} + h_q u_y^{(j)}}{h_q^2 + h_p^2} = \frac{1}{h_q^2 + h_p^2} u_q^{(j)}.$$

It follows immediately from the inequalities (40) that, for all $x \in (0, \lambda/2)$, $P_x^{(1)} > 0$ and $P_x^{(2)} < 0$. Given that, also from the previous proposition, $u_q^{(j)} = 0$ at the crest line $x = 0$ and at the trough line $x = \lambda/2$, we find that $P_x^{(j)} = 0$, $j = 1, 2$, along these lines. □

Also, directly from the Euler equation (3b), since $v^{(j)} = 0$ and $v_x^{(j)} < 0$ at $x = \lambda/2$, and in view of (7), it follows that $P_y^{(j)}(\lambda/2, y) < 0$, $j = 1, 2$. However, since $v_x^{(j)} > 0$ at $x = 0$, one has $P_y^{(j)}(0, y) > -g$ and therefore the sign for $P_y^{(j)}$ on the crest line $x = 0$ is indeterminate. Furthermore, since $P^{(1)} = P^{(2)}$ on the interface, we conclude that the pressure decreases strictly along the boundary of the fluid domain between the crest and the trough, from the lower left corner $(0, -h_2)$ to the top left corner $(0, h_1)$ in the anticlockwise direction (see Fig. 5).

Remark 4.1 It is known that the pressure within an irrotational fluid with a periodic, steady gravity wave, decreases along horizontal lines from the crest to the trough and

strictly increases with depth. In our framework, since we lack a constant interfacial pressure analogous to the atmospheric pressure along the free surface in a single layer fluid, we cannot guarantee the monotonicity of the pressure with depth in any of the layers. In the lower layer, although the pressure has a minimum on a point of the interface, we cannot extend this minimum to the entire interface and, in the upper layer, the fact that the pressure is superharmonic gives us no assurances as to the non-existence of a local maximum inside the fluid domain.

Proposition 4.2 *From the crest to the trough, i.e., for all* $x \in (0, \lambda/2)$, *along a streamline, there is a unique point* (x_0, y_0) *where the horizontal component of the velocity vanishes, i.e.* $u^{(j)}(x_0, y_0) = 0,\ j = 1, 2.$

Proof At the rigid lid and on the flat bottom, since there are no constant overlying or underlying currents, cf. (8), and taking into account that $u^{(j)}$ is even with respect to the variable x, it follows that

$$\int_0^{\lambda/2} u^{(1)}(x, h_1)\,\mathrm{d}x = 0 \quad \text{and} \quad \int_0^{\lambda/2} u^{(2)}(x, -h_2)\,\mathrm{d}x = 0.$$

Consequently, by the mean value theorem, and considering that $u_x^{(1)}(x, h_1) > 0$, for all $x \in (0, \lambda/2)$, at the rigid lid $y = h_1$ ($p = m_1/\rho_1$), there is a unique $x_1 \in (0, \lambda/2)$ such that $u^{(1)}(x_1, h_1) = 0$ and, furthermore,

$$u^{(1)}(0, h_1) < 0 < u^{(1)}(\lambda/2, h_1). \tag{41}$$

At the flat bottom $y = -h_2$ ($p = -m_2/\rho_2$), following the same reasoning as above and taking into account that $u_x^{(2)}(x, -h_2) < 0$ for all $x \in (0, \lambda/2)$, there is a unique $x_2 \in (0, \lambda/2)$ such that $u^{(2)}(x_2, -h_2) = 0$ and

$$u^{(2)}(\lambda/2, -h_2) < 0 < u^{(2)}(0, -h_2). \tag{42}$$

Now, by Proposition 4.1, the horizontal component of the velocity $u^{(1)}$ is strictly increasing (as a function of x) along every streamline $\psi^{(1)} = -p$, $0 \le p \le m_1/\rho_1$. Moreover, taking into account the inequalities (22) and (41), we can see that

$$\forall_{y\in[\eta(0),h_1]}\ \ u^{(1)}(0, y) < 0 \qquad \text{and} \qquad \forall_{y\in[\eta(\lambda/2),h_1]}\ \ u^{(1)}(\lambda/2, y) > 0$$

and, consequently, from the crest to the trough, there is a unique point along the streamline $\psi^{(1)} = -p$ where $u^{(1)}$ vanishes. Similarly, since the horizontal component of the velocity $u^{(2)}$ is strictly decreasing (as a function of x) along every streamline $\psi^{(2)} = -p$, $-m_2/\rho_2 \le p \le 0$, considering inequalities (22) and (42), we conclude that

$$\forall_{y\in[-h_2,\eta(0)]}\ \ u^{(2)}(0, y) > 0 \qquad \text{and} \qquad \forall_{y\in[-h_2,\eta(\lambda/2)]}\ \ u^{(2)}(\lambda/2, y) < 0$$

and thus, from the crest to the trough, there is a unique point along the streamline $\psi^{(2)} = -p$ where $u^{(2)}$ is equal to 0. □

Note that, for each streamline $\psi^{(1)} = -p,\ p \in [0, m_1/\rho_1]$, there is a unique $q \in (0, c\lambda/2)$ where $u^{(1)}$ vanishes and for each streamline $\psi^{(2)} = -p,\ p \in [-m_2/\rho_2, 0]$, there is a unique $q \in (0, c\lambda/2)$ where $u^{(2)}$ vanishes. In view of the inequalities (40), the implicit function theorem guarantees that, from the crest to the trough, the curves where $u^{(1)} = 0$ and $u^{(2)} = 0$ are smooth, cf. [31].

Proposition 4.3 *From the crest to the trough, i.e., for all* $x \in (0, \lambda/2)$,

1. *The slope of a streamline is strictly decreasing in depth, for all* $y \in (\eta(x), h_1)$.
2. *The slope of a streamline is strictly increasing in depth, for all* $y \in (-h_2, \eta(x))$.

Proof Given a streamline parametrized by $x \mapsto (x, \gamma(x))$, where γ is a differentiable function, by Eq. (37), we have

$$\gamma' = \frac{v^{(j)}}{u^{(j)} - c}, \quad j = 1, 2.$$

Therefore, the derivative with respect to the y variable of the slope of the streamline is

$$\partial_y \gamma' = \frac{v_y^{(j)}(u^{(j)} - c) - u_y^{(j)} v^{(j)}}{(u^{(j)} - c)^2} = \frac{-u_x^{(j)}(u^{(j)} - c) - u_y^{(j)} v^{(j)}}{(u^{(j)} - c)^2}$$

$$= u_q^{(j)} \frac{(u^{(j)} - c)^2 + (v^{(j)})^2}{(u^{(j)} - c)^2}.$$

Consequently, in view of the inequalities (40), it follows that

$$\partial_y \gamma' > 0 \quad \text{in } \{(x, y) \in \mathbb{R}^2 : 0 < x < \lambda/2 \wedge \eta(x) < y < h_1\}$$

and

$$\partial_y \gamma' < 0 \quad \text{in } \{(x, y) \in \mathbb{R}^2 : 0 < x < \lambda/2 \wedge -h_2 < y < \eta(x)\}.$$

□

In the moving frame, observing that the vertical displacement of a particle travelling along a streamline parametrized by $x \mapsto (x, \gamma(x))$ is given by

$$-\int_0^{\lambda/2} \gamma'(x)\, \mathrm{d}x$$

one can conclude that it decreases with the distance to the interface, decreasing with depth in the lower layer and increasing in the upper layer, as can be seen in Fig. 6.

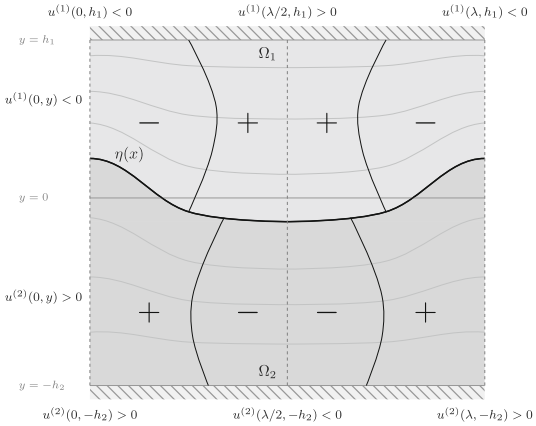

Fig. 6 The zero level set of the function $u^{(j)}$ intersecting the streamlines describing the motion of the fluid

4.2 Particle Paths

It is known from [25] that, in the absence of underlying currents, there are no closed particle paths in an irrotational fluid under a periodic travelling wave propagating at the surface over a flat bed. Here, based on the properties of the velocity field components proved above, we build a pictorial description of the particle paths in both layers of the fluid.

In the moving frame, the physical path of a particle is, in each layer, a solution of the system

$$\begin{cases} \left(x^{(j)}\right)'(t) = u^{(j)}(x,y) - c \\ \left(y^{(j)}\right)'(t) = v^{(j)}(x,y) \end{cases}, \quad j = 1,2\,.$$

In view of (24), we can easily see that a solution of the previous system lies on the level set of the stream function $\psi^{(j)}$, i.e.

$$\partial_t \psi^{(j)}(x(t),y(t)) = -v^{(j)}(u^{(j)}-c) + (u^{(j)}-c)v^{(j)} = 0.$$

Defining the *elapsed time of a particle* $\theta^{(j)}$ by the time a particle takes to traverse one period of the wave along a streamline $\psi^{(j)} = -p$ in the moving frame, we have

$$\theta^{(j)}(p) = \int_0^\lambda \frac{\mathrm{d}x}{c - u^{(j)}(x,y(x))}, \quad j = 1,2,$$

and assuming that there is no constant underlying current on the flat bottom and no overlying current on the rigid lid, following [25], it is straightforward to conclude that

$$\theta^{(j)}(p) > \frac{\lambda}{c}, \quad j = 1,2. \tag{43}$$

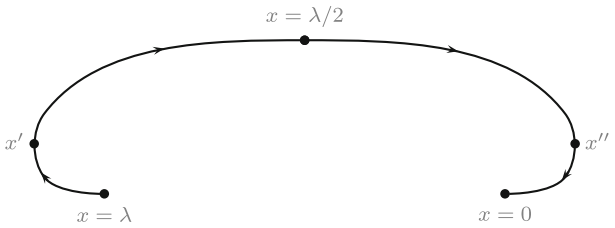

Fig. 7 Trajectory of a particle moving in the upper layer, with $x' \in (\lambda/2, \lambda)$ and $x'' \in (0, \lambda/2)$

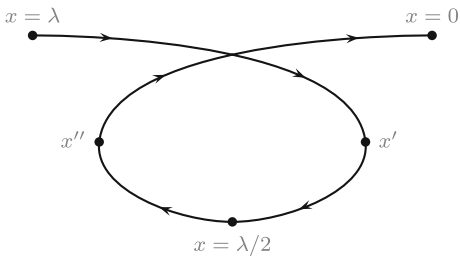

Fig. 8 Trajectory of a particle moving in the lower layer, with $x' \in (\lambda/2, \lambda)$ and $x'' \in (0, \lambda/2)$

Now, defining the *drift* of a particle as the horizontal distance moved by a particle between its positions at two consecutive crest lines, it can be given by

$$c\,\theta^{(j)} - \lambda.$$

In view of (43), we conclude that the *drift* is positive, which means that the particle moves in the direction of the propagation of the wave. Consequently, there are no closed particle paths in the upper and lower layers.

In the upper layer, for a particle located at the point (λ, y), $y \in [\eta(\lambda), h_1)$, considering the Proposition 4.2 (see Fig. 6), the inequalities (18) and the monotonic properties of the functions $u^{(j)}$ and $v^{(j)}$ with respect to the x variable, one can see that it moves according the line depicted in Fig. 7. However, in the lower layer, taking a particle located at the point (λ, y), $y \in (-h_2, \eta(\lambda)]$, we can observe that it moves according to the line depicted in Fig. 8.

It is known from [30] that for the case of a single layer fluid the *drift* of every particle strictly decreases with depth. In our framework, it can be shown in a similar way that

$$\partial_p^2 \theta^{(j)} > 0, \quad j = 1, 2,$$

and

$$\partial_p \theta^{(1)}(m_1/\rho_1) = 0, \quad \partial_p \theta^{(2)}(-m_2/\rho_2) = 0.$$

Consequently, we can conclude that in the upper layer the *drift* increases with depth, from the top rigid lid to the interface, and in the lower layer the *drift* decreases with depth, from the interface to the flat bottom.

5 Conclusions

In this article we considered a periodic travelling irrotational wave propagating at the interface between two homogeneous, incompressible and inviscid fluids bounded above by a rigid lid and below by a flat bottom. In this study it was assumed that the horizontal component of the velocity field is smaller than the wave speed, therefore excluding highest waves.

For interfacial waves of small amplitude, where linear water waves theory can apply, we presented an explicit expression for the interface wave profile depending on the pressure measurements at the rigid lid and at the flat bottom. For the general non-linear case, we were able to derive a lower bound for the interfacial wave height.

Under certain conditions imposed on the horizontal velocity of the motion at the interface, we were also able to generalize the results from Constantin and Strauss [30] to a two-layer fluid, showing that, along the streamlines, from crest to trough, the horizontal component of the velocity field increases strictly in the upper layer and decreases strictly in the lower layer. We also proved that the pressure decreases strictly along the boundary of the fluid domain between the crest and the trough, from the lower left corner to the top left corner, in the anticlockwise direction.

We studied the properties of the components of the velocity field and analysed the dependence of the slope of the streamlines on the fluid depth, concluding that the vertical displacement of a particle travelling along a streamline decreases with the distance to the interface, decreasing with depth in the lower layer and increasing in the upper layer.

Finally, based on the behavior of the velocity field components, we obtained the particle paths for the particles of both layers, with a positive *drift* (in the case of no underlying or overlying current), which is null at both top and lower boundaries, but increases towards the interface to a maximum value. It is found that particle paths are not closed as in the linear case, where they are elliptical in shallow water and circular in deep water (see e.g. [32]), but loop forward, with a positive drift, in both layers.

Acknowledgements F. S. Cal was partially supported by FCT Fundação para a Ciência e a Tecnologia, Portugal, through the project UIDB/04674/2020 (CIMA). G. A. S. Dias received no funding for this work. The authors state, moreover, no conflict of interest in the making of this work.

Author Contributions In this work, there was no special contribution by any author that differs from that of the other. Both G.D. and F.C. worked in tandem.

Funding Open access funding provided by FCT|FCCN (b-on).

Data Availability No datasets were generated or analysed during the current study.

Declarations

Conflict of interest The authors state no conflict of interest in the making of this work.

References

1. Kotchine, N.: Détermination rigoureuse des ondes permanentes d'ampleur finie à la surface de séparation de deux liquides de profondeur finie. Math. Ann. **98**(1), 582–615 (1928). https://doi.org/10.1007/BF01451610
2. Levi-Civita, T.: Détermination rigoureuse des ondes permanentes d'ampleur finie. Math. Ann. **93**(1), 264–314 (1925). https://doi.org/10.1007/BF01449965
3. Struik, D.J.: Détermination rigoureuse des ondes irrotationelles périodiques dans un canal à profondeur finie. Math. Ann. **95**(1), 595–634 (1926). https://doi.org/10.1007/BF01206629
4. Holyer, J.Y.: Large amplitude progressive interfacial waves. J. Fluid Mech. **93**, 433–448 (1979). https://doi.org/10.1017/S0022112079002585
5. Meiron, D.I., Saffman, P.G.: Overhanging interfacial gravity waves of large amplitude. J. Fluid Mech. **129**, 213–218 (1983). https://doi.org/10.1017/S0022112083000737
6. Sun, S.M.: Existence of large amplitude periodic waves in two-fluid flows of infinite depth. SIAM J. Math. Anal. **32**(5), 1014–1031 (2001). https://doi.org/10.1137/S0036141099352728
7. Camassa, R., Rusås, P.-O., Saxena, A., Tiron, R.: Fully nonlinear periodic internal waves in a two-fluid system of finite depth. J. Fluid Mech. **652**, 259–298 (2010). https://doi.org/10.1017/S0022112010000054
8. Choi, W., Camassa, R.: Fully nonlinear internal waves in a two-fluid system. J. Fluid Mech. **396**, 1–36 (1999). https://doi.org/10.1017/S0022112099005820
9. Maklakov, D.V., Sharipov, R.R.: Almost limiting configurations of steady interfacial overhanging gravity waves. J. Fluid Mech. **856**, 673–708 (2018). https://doi.org/10.1017/jfm.2018.721
10. Guan, X., Vanden-Broeck, J.-M., Wang, Z.: New solutions for periodic interfacial gravity waves. J. Fluid Mech. **928**, 5 (2021). https://doi.org/10.1017/jfm.2021.854
11. Drennan, W.M., Kahma, K.K., Donelan, M.A.: The velocity field beneath wind-waves—observations and inferences. Coast. Eng. **18**(1), 111–136 (1992). https://doi.org/10.1016/0378-3839(92)90007-H
12. Tsai, C.-H., Huang, M.-C., Young, F.-J., Lin, Y.-C., Li, H.-W.: On the recovery of surface wave by pressure transfer function. Ocean Eng. **32**(10), 1247–1259 (2005). https://doi.org/10.1016/j.oceaneng.2004.10.020
13. Escher, J., Schlurmann, T.: On the recovery of the free surface from the pressure within periodic traveling water waves. J. Nonlinear Math. Phys. **15**(sup2), 50–57 (2008). https://doi.org/10.2991/jnmp.2008.15.s2.4
14. Clamond, D., Constantin, A.: Recovery of steady periodic wave profiles from pressure measurements at the bed. J. Fluid Mech. **714**, 463–475 (2013). https://doi.org/10.1017/jfm.2012.490
15. Constantin, A.: Estimating wave heights from pressure data at the bed. J. Fluid Mech. **743**, 2 (2014). https://doi.org/10.1017/jfm.2014.81
16. Vasan, V., Oliveras, K.L., Henderson, D.M., Deconinck, B.: A method to recover water-wave profiles from pressure measurements. Wave Motion **75**, 25–35 (2017). https://doi.org/10.1016/j.wavemoti.2017.08.003
17. Oliveras, K.L., Vasan, V., Deconinck, B., Henderson, D.: Recovering the water-wave profile from pressure measurements. SIAM J. Appl. Math. **72**(3), 897–918 (2012). https://doi.org/10.1137/110853285
18. Bonneton, P., Lannes, D., Martins, K., Michallet, H.: A nonlinear weakly dispersive method for recovering the elevation of irrotational surface waves from pressure measurements. Coast. Eng. **138**, 1–8 (2018). https://doi.org/10.1016/j.coastaleng.2018.04.005
19. Basu, B.: Estimation of wave heights from pressure data at the bed in the presence of uniform underlying currents. Nonlinear Anal. **156**, 82–89 (2017). https://doi.org/10.1016/j.na.2017.01.016
20. Basu, B.: Wave height estimates from pressure and velocity data at an intermediate depth in the presence of uniform currents. Philos. Trans. A Math. Phys. Eng. Sci. **376**(2111), 20170087 (2018). https://doi.org/10.1098/rsta.2017.0087

21. Marino, M., Rabionet, I.C., Musumeci, R.E.: Measuring free surface elevation of shoaling waves with pressure transducers. Cont. Shelf Res. **245**, 104803 (2022). https://doi.org/10.1016/j.csr.2022.104803
22. Murashige, S., Choi, W.: Two-dimensional stability analysis of finite-amplitude interfacial gravity waves in a two-layer fluid. J. Fluid Mech. **938**, 13 (2022). https://doi.org/10.1017/jfm.2022.145
23. Li, Q., Fečkan, M., Wang, J.: On the estimation of wave heights for periodic water waves from velocity and pressure data. Results Phys. **51**, 106678 (2023). https://doi.org/10.1016/j.rinp.2023.106678
24. Constantin, A., Villari, G.: Particle trajectories in linear water waves. J. Math. Fluid Mech. **10**, 1–18 (2008). https://doi.org/10.1007/s00021-005-0214-2
25. Constantin, A.: The trajectories of particles in stokes waves. Invent. Math. **166**, 523–535 (2006). https://doi.org/10.1007/s00222-006-0002-5
26. Umeyama, M., Matsuki, S.: Measurements of velocity and trajectory of water particle for internal waves in two density layers. Geophys. Res. Lett. **38**(3) (2011). https://doi.org/10.1029/2010GL046419
27. Borluk, H., Kalisch, H.: Particle dynamics in the KdV approximation. Wave Motion **49**(8), 691–709 (2012). https://doi.org/10.1016/j.wavemoti.2012.04.007
28. Bjørnestad, M., Buckley, M., Kalisch, H., Streßer, M., Horstmann, J., Frøysa, H.G., Ige, O.E., Cysewski, M., Carrasco-Alvarez, R.: Lagrangian measurements of orbital velocities in the surf zone. Geophys. Res. Lett. **48**(21) (2021) https://doi.org/10.1029/2021GL095722
29. Cal, F.S., Dias, G.A.S.: Velocity and energy of periodic travelling interfacial waves between two bounded fluids. Wave Motion **123**, 103232 (2023). https://doi.org/10.1016/j.wavemoti.2023.103232
30. Constantin, A., Strauss, W.: Pressure beneath a stokes wave. Commun. Pure Appl. Math. **63**, 533–557 (2010). https://doi.org/10.1002/cpa.20299
31. Constantin, A.: The flow beneath a periodic travelling surface water wave. J. Phys. A **48**(25), 143001 (2015). https://doi.org/10.1088/1751-8113/48/14/143001
32. Kundu, P.K., Cohen, I.M., Dowling, D.R.: Fluid Mechanics, 5th edn. Academic Press, Boston (2012). https://doi.org/10.1016/C2009-0-63410-3